Time-dependent quantum study of H(2S) + FO(2π) → OH(2π) + F(2P) reaction on the 1 3A′ and 13A″ states

ARTICLE *in* JOURNAL OF COMPUTATIONAL CHEMISTRY · NOVEMBER 2010

Impact Factor: 3.59 · DOI: 10.1002/jcc.21555 · Source: PubMed

3 AUTHORS, INCLUDING:

Fahrettin Gogtas

Yıldırım Beyazıt Üniversitesi

24 PUBLICATIONS **100** CITATIONS

SEE PROFILE

Mustafa Kurban

Middle East Technical University

6 PUBLICATIONS **1** CITATION

SEE PROFILE

Time-Dependent Quantum Study of $H(^2S) + FO(^2\Pi) \rightarrow OH(^2\Pi) + F(^2P)$ Reaction on the $1^3A'$ and $1^3A''$ States

FAHRETTIN GOGTAS,[1] RUKIYE TUTUK,[1] MUSTAFA KURBAN[2]
[1] *Faculty Science and Arts, Department of Physics, Firat University, Elaziğ, Turkey*
[2] *Department of Physics, Muş Alparslan University, Muş, Turkey*

Received 3 September 2009; Revised 28 February 2010; Accepted 3 March 2010
DOI 10.1002/jcc.21555
Published online 17 May 2010 in Wiley Online Library (wileyonlinelibrary.com).

Abstract: The dynamics of the $H(^2S)+FO(^2\Pi) \rightarrow OH(^2\Pi)+F(^2P)$ reaction on the adiabatic potential energy surface of the $1^3A'$ and $1^3A''$ states is investigated. The initial state selected reaction probabilities for total angular momentum $J = 0$ have been calculated by using the quantum mechanical real wave packet method. The integral cross sections and initial state selected reaction rate constants have been obtained from the corresponding $J = 0$ reaction probabilities by means of the simple J-Shifting technique. The initial state-selected reaction probabilities and reaction cross section do not manifest any sharp oscillations and the initial state selected reaction rate constants are sensitive to the temperature.

 J Comput Chem 31: 2607–2611, 2010

Key words: reactive scattering; quantum wavepacket study; reaction probabilities; cross sections; rate constant

Introduction

The OHF system has been given much attention in recent years due to its contribution to the catalytic destruction cycle.[1–4] The quantum mechanical studies on this system require three-dimensional coupled potential energy surfaces, which require high level *ab initio* calculations. Recently, global potential energy surfaces for several electronic states of OHF have been reported. Gómez-Carrasco et al.[5] performed high-level MRCI electronic structure calculations for 8069 energy points to calibrate the fitted potential energy surface (PES) of the ground adiabatic $1^3A''$ triplet electronic state. Quasi-classical trajectory (QCT) and wave packet studies[5–7] of $F(^2P) + OH(^2\Pi) \rightarrow O(^3P) + HF(^1\Sigma^+)$ reaction have been performed on this high-quality triplet PES and a subsequent improved version.[6] Quantum state-to-state calculation[8] of the same reaction were repeated by using a newly proposed coordinate transformation method in conjunction with the Coriolis-coupled (CC) method. Recently, the reverse reaction, $H(^2S) + FO(^2\Pi) \rightarrow OH(^2\Pi) + F(^2P)$ has been subject to many studies. Gogtas[9] has carried out the quantum real wave packet calculations of the reverse reaction on the ground $^3A''$ potential energy surface. The same reaction has been studied by Zhao et al.[10] by using QCT method. Most recently, a comparative dynamics study for the title reaction with both product channels of $OH(^2\Pi) + F(^2P)$ and $HF(^1\Sigma^+) + O(^3P)$ have been carried out by QCT and time-dependent quantum wave packet calculations on the same surface.[11]

The OHF system can also provide the opportunity to perform a nonadiabatic study with the coupled electronic states involved. For this reason, Gomez-Carrasco et al.[12,13] further reported several coupled diabatic potential energy surfaces ($1^3A''$, $2^3A''$, and $1^3A'$) and extended their previous dynamics study of the $F(^2P)+OH(^2\Pi) \rightarrow O(^3P) + HF(^1\Sigma^+)$ reaction by wave packet calculations implemented with the centrifugal sudden (CS) approximation on the excited $2^3A''$ and $1^3A'$ triplet states. Later, the PESs[14] for the first five singlet states of the OHF system have been constructed from *ab initio* electronic structure calculations at the MRCI level. The ground adiabatic $1^1A'$ singlet PES was then used in the both quasi-classical trajectory and the wave packet calculations[15] of $O(^1D) + HF(^1\Sigma^+) \rightarrow F(^2P) + OH(^2\Pi)$.

In this study, we have performed three-dimensional real wave packet calculations of the reaction probabilities at zero total angular momentum for the $H(^2S)+FO(^2\Pi) \rightarrow OH(^2\Pi)+F(^2P)$ reaction based on the $1^3A'$ and $1^3A''$ state potential energy surfaces.[12] The simple J-Shifting method is used to compute the reaction probabilities for $J > 0$. The total reactive cross-sections are calculated by summing the partial probabilities over all J values and the initial state selected rate constants are calculated by Boltzmann averaging the integral cross sections.

Correspondence to: F. Gogtas; e-mail: fgogtas@firat.edu.tr

Theory

The time-dependent real wave packet approach of Gray and Balint-Kurti[16] is an efficient and accurate method for solving the time dependent Schrödinger equation. The method is based on the solution of a modified Schrödinger equation given as

$$\mathbf{i}\hbar\frac{\partial\Psi(R,r,\theta,t)}{\partial t} = f(\hat{H})\Psi(R,r,\theta,t) \tag{1}$$

where $f(\hat{H})$ is defined in terms of the Hamiltonian operator. The functional mapping of the Hamiltonian operator allows the propagation of the wave packet to be achieved by a Chebyshev iterative method where each step requires a single evaluation of the action of the Hamiltonian on the real part of the wave packet follows.[16–19]

$$q_{n+1} = \hat{A}(-\hat{A}q_{n-1} + 2\hat{H}_s q_n) \tag{2}$$

where n is the iteration step, q is the real part of the wave function (ψ) represented on discrete grid points, $q = Re\{\psi\}$ and $\hat{A}$ is some appropriate operator, which damps the wavepacket amplitude as it approaches the grid edges.[20] Thus, the computational time is reduced two times as compared to the propagation of complex wave packet. The wave packet propagation may be performed either in terms of reactant or product Jacobi coordinates. In this article, the product Jacobi coordinates R, r, and γ are used with R being the F to OH centre of mass distance, r being the OH internuclear distance and γ being the angle between two vectors associated with R and r. The wave packet is represented with evenly spaced grids in R and r, and a Legendre basis set in $\cos(\gamma)$.The evaluation of the kinetic energy term associated with R and r is accomplished using the dispersion fitted finite difference method.[21] The angular part of the wave packet is represented using discrete variable representation(DVR) based on Gauss-Legendre Quadrature points. The DVR method is then used to evaluate the action of angular kinetic energy operator on the wave function.[22]

In this study, the wave packet calculations are performed at zero total angular momentum quantum number ($J = 0$). The initial wave function has been set up as described by Hankel et al.[23] The initial wave function was first calculated in reactant Jacobi coordinates in the asymptotic region of the entrance channel and then transformed to the product coordinates before the propagation started. The transformation of the wave function from reactant coordinates to product coordinates has been described by Gray and Balint-Kurti in all details.[16] Equation (2) is then solved for many iteration steps until the wave function has completely left the interaction region. The wave packet is analyzed in the asymptotic region of the product channel at $R = R_\infty$. The reaction probability for the production of a specific final vibrational–rotational state from a specified initial reactant level is given by[24]:

$$P^{J=0}_{v',j',v,j}(E) = \left(\frac{\hbar^2 a_s}{\tau\left(1-E_s^2\right)^{1/2}}\right)^2 \left(\frac{k_{v',j'}k_{v,j}}{\mu_{A+BC}\mu_{AB+C}}\right)\left|\frac{2A_{v',j',v,j}(f)}{g(-k_{v,j})}\right|^2 \tag{3}$$

where τ is time step, $E_s = a_s E + b_s$. $A_{v',j',v,j}(f)$ are the discrete Fourier transform of the projection coefficients calculated on the analysis line (see details in ref. 16) whereas $g(-k_{v,j})$ is the Fourier transform of initial Gaussian. The calculation of the integral cross sections as a function of the collision energy for each rovibrational state v,j of the reagent molecule requires summing up all the partial waves. As the reaction under study is dominated by a barrier, the simple J-shifting method of Bowman[25,26] is used to estimate the reaction probabilities for total angular momentum values $J > 0$. The total cross sections are thus calculated[27]

$$\sigma_{v,j}(E) = \frac{\pi}{k^2_{v,j}}\frac{1}{2j+1}\sum_{J=0}^{\infty}(2J+1)P^J_{v,j}(E) \tag{4}$$

The initial state selected rate constant are calculated by Boltzmann averaging the corresponding integral cross section over the translational energy[28]

$$k_{jv}(T) = \sqrt{\frac{8k_BT}{\pi\mu_{A-BC}}}(k_BT)^{-2}\int E_C\sigma_{vj}(E_C)e^{-E_C/k_BT}dE_C \tag{5}$$

where k_B is the Boltzmann constant and $E_C = E - \epsilon_{\mu,j}$ is the collision energy.

Results and Discussion

In this section, we have calculated the initial state selected reaction probabilities, integral cross sections and initial state selected rate constants for the $H(^2S) + FO(^2\Pi) \rightarrow OH(^2\Pi) + F(^2P)$ reaction for the initial quantum state $v = 0, j = 0$. Three-dimensional adiabatic potential energy surfaces (PES) for the $1^3A'$ and $1^3A''$ states[7] have been used in the calculations. The minimum energy paths of the two states for the $H(^2S) + FO(^2\Pi) \rightarrow OH(^2\Pi) + F(^2P)$ reaction are shown in Figure 1. The zero of the energy is set up to the reactant asymptote. As it may be seen from the figure that both states show well described reactant and product channels. $1^3A'$ surface shows a barrier of 0.38 eV in the entrance channel at a configuration $r_{oh} = 2.92$ a.u., $r_{fo} = 2.73$ a.u., and $\theta = 179^o$. The

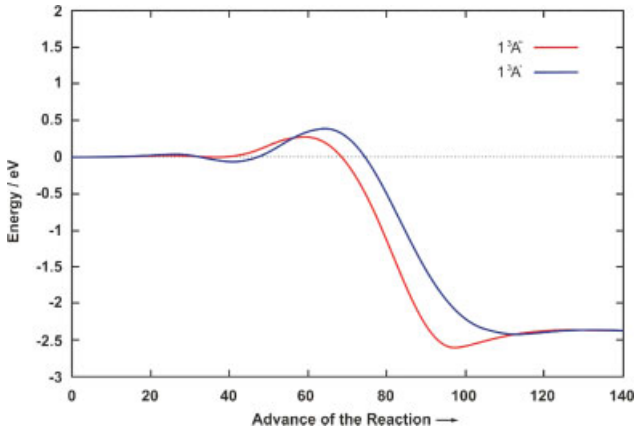

Figure 1. The minimum energy paths of the $1^3A'$ and $1^3A''$ states for the $H(^2S) + FO(^2\Pi) \rightarrow OH(^2\Pi) + F(^2P)$ reaction.

Table 1. The Most Relevant Parameters Used for Calculations.

Variable	Value	Description
j_{max}	120	Number of angular basis functions
N_R	300	Number of points in the R grid
R_{min}	0	Minimum value of R grid
R_{max}	13	Maximum value of R grid
N_r	160	Number of points in the r grid
r_{min}	0.5	Minimum value of r grid
r_{max}	10	Maximum value of r grid
σ	15	Width parameter of initial wavepacket
E_0	0.4	Initial kinetic energy of wavepacket
$R_{\alpha,0}$	7.0	Location of centre of wavepacket at $t = 0$

All parameters are given in atomic units.

exit channel presents a shallow well of −2.40 eV below the reactant asymptote, located at a configuration $r_{oh} = 1.837$ a.u., $r_{fo} = 5.21$ a.u., and $\theta = 180^o$, and the reaction is exoergic of 2.36 eV. There is also a well of −0.04 eV in the entrance channel at the configuration $r_{oh} = 4.61$ a.u., $r_{fo} = 2.59$ a.u. On the other hand, $1^3A''$ surface shows a barrier of 0.265 eV in the entrance channel at a configuration $r_{oh} = 3.214$ a.u., $r_{fo} = 2.707$ a.u., and $\theta = 123.3^o$. The exit channel presents a shallow well of −2.59 eV below the reactant asymptote, located at a configuration $r_{oh} = 1.864$ a.u., $r_{fo} = 3.561$ a.u., and $\theta = 93.5^o$, and the reaction is exoergic of 2.36 eV.

The initial wave packet centered around R_0 in the entrance valley was given an initial kinetic energy of 0.4 eV. Equation (2) was then solved by propagating the the real part of the wavepacket forwards in time in many relatively small steps, as outlined above. At each time step, the wave function was analyzed at an analysis plane located in the asymptotic region of product channel. An absorbing potential in exponential form was used at the edges of the grid to avoid the reflection of the wave packet from the end of the grid. A time step of 2.3 fs was used for the propagation. To test the convergence of the results, many calculations were carried out. $N_R = 300$, $N_r = 160$, and $N_j = 120$ were found to give converged results. The propagation time that was found to be sufficient to converge the reaction probabilities was 20,000 a.u. (483 fs). The values of the various grid parameters used in the calculations are shown in Table 1. These parameters were adopted after several tests so as to get the converged results.

Figure 2 shows the state-to-state reaction probabilities as a function of collision energy for $H + FO(v = 0, j = 0) \rightarrow OH(v' = 0, j') + F$ reaction. As it may be seen from the figure that the reaction probabilities show similar variations as a function of the energy for different final rotational quantum states. That is, the probabilities show no clear dependency to final rotational quantum states. All state-to-state probabilities show a background shape with some oscillations located in the high energy region and slightly increase with increasing final rotational quantum number. Figure 3 shows the state-to-state reaction probabilities summed over all final rotational states as a function of total energy for $H + FO(v = 0, j = 0) \rightarrow OH(v') + F$ reaction. It may be seen from the figure that as the reaction probabilities summed over all final rotational states, all broad oscillations in the probabilities disappears and the probabilities increase with increasing final vibrational state.

Figure 4 shows the reactive scattering probabilities summed over all final states for the reaction corresponding to the FO reactant in its $v = 0; j = 0$ state for both $1^3A'$ and $1^3A''$ states. As it may be seen from the figure that the total quantum reaction probabilities for $1^3A'$ show a reaction threshold of 0.38 eV whereas those for $1^3A''$ show a threshold at 0.2 eV. The probabilities for both states increase with the increasing collision energy. As the locations of the barriers for both states are compared, the $1^3A''$ has an earlier barrier and the height of the barrier for this state is much lower. The threshold behaviors are consistent with the energy barrier along the minimum energy path of the reaction system, which indicates a direct mechanism. The reaction probabilities over all collision energy range for the $1^3A''$ are higher than those for $1^3A'$ state. This is also consistent with the heights of energy barriers for two states.

The most widely studied reaction based on the same potential energy surface is $F(^2P) + OH(^2\Pi) \rightarrow O(^3P) + HF(^1\Sigma^+)$ reaction, which is exoergic, there is a well of 0.00845 a.u. in the reactant channel, and a well in the product channel of 0.0583 a.u. below the reactant asymptote. The transition state is located at an energy of 0.00025 a.u. above the reactant asymptote, showing

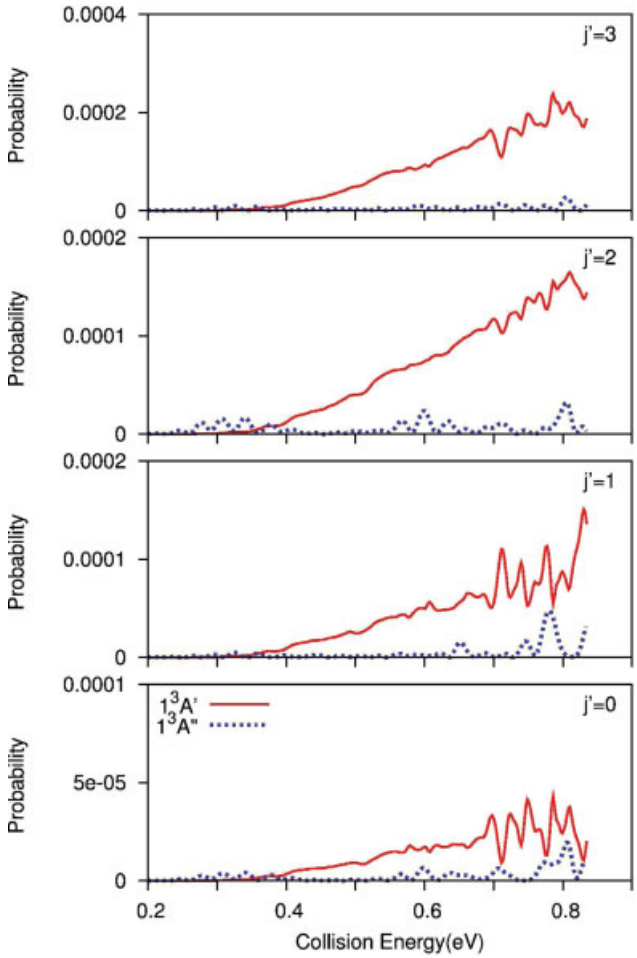

Figure 2. The reaction probabilities for $H(^2S) + FO(^2\Pi)(v = 0, j = 0) \rightarrow OH(^2\Pi)(v' = 0, j') + F(^2P)$ reaction plotted as a function of collision energy.

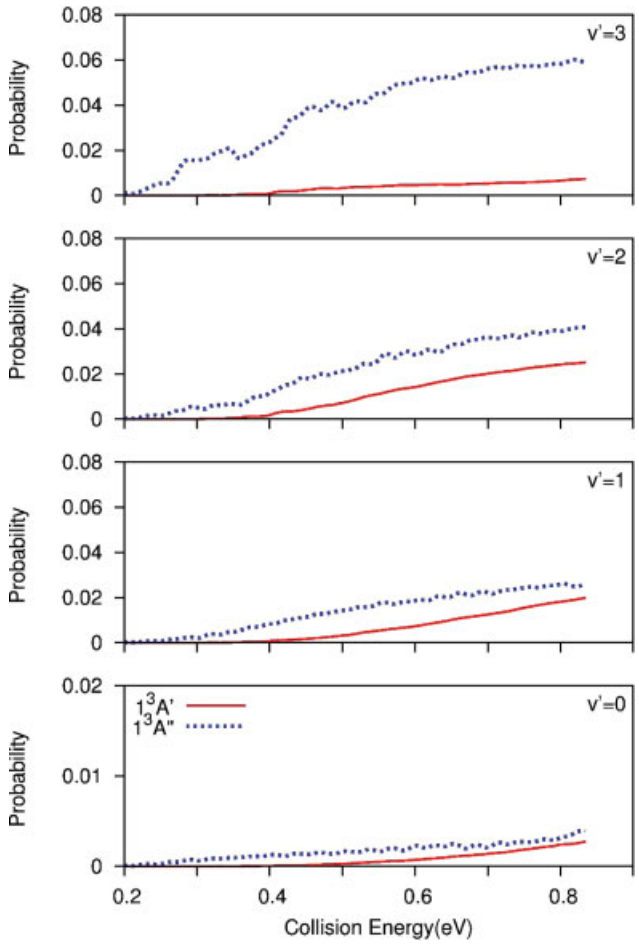

Figure 3. The reaction probabilities for $H(^2S) + FO(^2\Pi)(v = 0, j = 0) \rightarrow OH(^2\Pi)(v') + F(^2P)$ summed over all final rotational states as a function of collision energy. [Color figure can be viewed in the online issue, which is available at wileyonlinelibrary.com.]

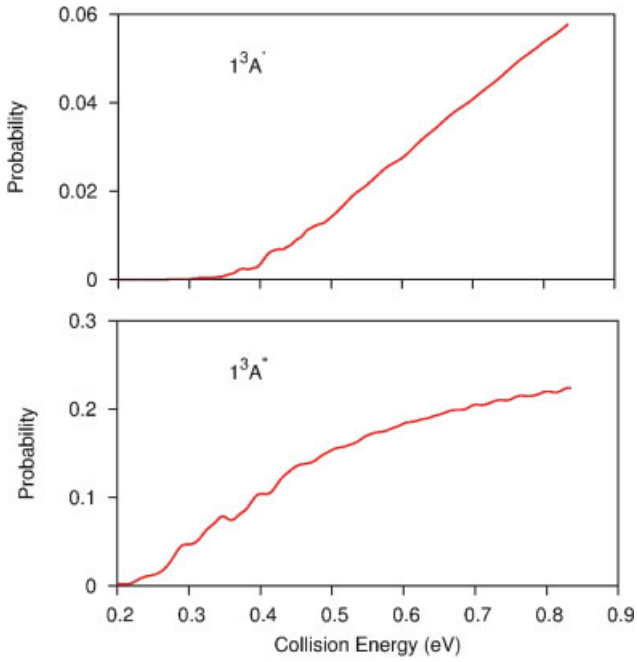

Figure 4. Reaction probabilities for $H(^2S)+FO(^2\Pi)(v = 0, j = 0) \rightarrow OH(^2\Pi)+F(^2P)$ summed over all final rovibrational states as a function of collision energy. [Color figure can be viewed in the online issue, which is available at wileyonlinelibrary.com.]

that the reaction has practically no nominal barrier. Therefore, the reaction probability for this reaction has not shown any threshold behavior. The topographic features of the $H(^2S) + FO(^2\Pi) \rightarrow OH(^2\Pi) + F(^2P)$ and $F(^2P) + OH(^2\Pi) \rightarrow O(^3P) + HF(^1\Sigma^+)$ reactions are very similar, except that our reaction has an effective barrier (0.265 eV for $1^3A'$ and 0.38 eV for $1^3A''$) located in the reactant channel. Therefore, the threshold behavior presented by our reaction is due to the existence of the early barrier in the entrance channel.

Figure 5 shows the integral cross sections, or excitation functions, for both $1^3A'$ and $1^3A''$ states corresponding to the *FO* reactant in its $v = 0, j = 0$ initial state. The total reactive cross sections for $1^3A'$ and $1^3A''$ states show threshold at collision energy of 0.38 eV and 0.2 eV, respectively, and increase gradually with relative translational energy. Again, the cross sections for both states do not manifest any resonance structures as the potential energy surface has not shown a deep well in the entrance channel. As it is expected, the cross sections over all collision energy range for the $1^3A''$ are higher than those for $1^3A'$ state. The initial state selected $H + FO(v = 0, j = 0)$ rate constant is displayed in Figure 6 for

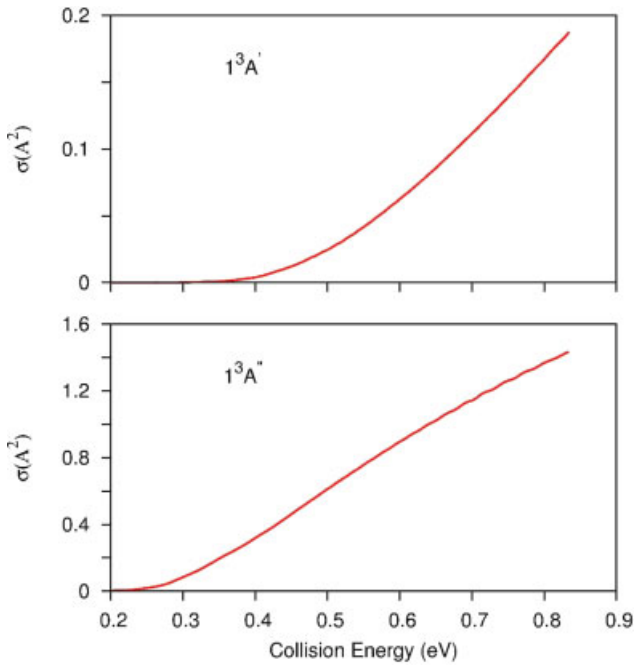

Figure 5. Integral cross-sections for the $H(^2S) + FO(^2\Pi)(v = 0, j = 0)$ reaction. [Color figure can be viewed in the online issue, which is available at wileyonlinelibrary.com.]

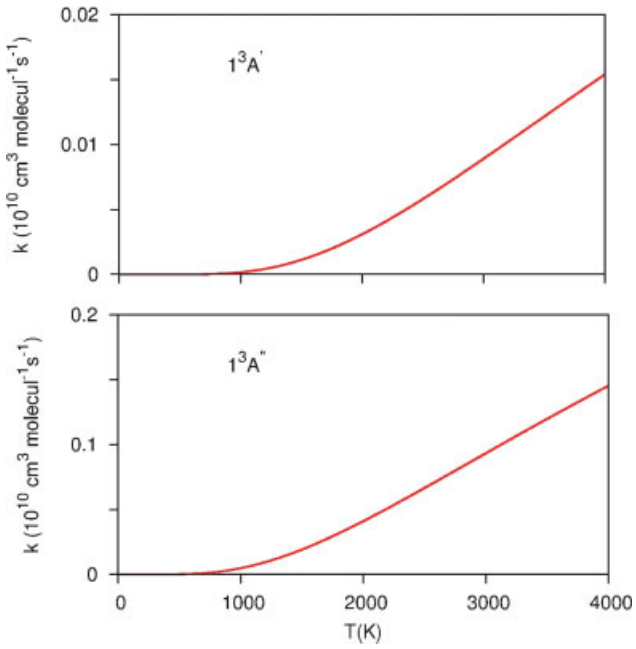

Figure 6. Initial state selected rate constant for the $H(^2S) + FO(^2\Pi)(v = 0, j = 0)$ derived from the integral cross sections in Figure 5. [Color figure can be viewed in the online issue, which is available at wileyonlinelibrary.com.]

the *FO* in its ground state. The rate constant calculated in this study increases sharply with temperature. The features shown here in the reaction probabilities and the integral cross sections predicted a dominant role of the early energy barrier in mediating the underlying reaction mechanisms. In addition, the larger cross sections of the $1^3A''$ than of $1^3A'$ indicates that the formation of the product is much easier on the $1^3A''$ state as compared to $1^3A'$.

Conclusion

Three-dimensional quantum reel wave packet calculations for the $H(^2S) + FO(^2\Pi) \rightarrow OH(^2\Pi) + F(^2P)$ reaction on the ground $1^3A''$ and $1^3A'$ potential energy surfaces have been performed. The probabilities are strongly dependent on the translational energy and final vibrational quantum states but less on final rotational states. The integral cross section and the initial state selected reaction rate constant have also been calculated. The calculations showed that total reaction probabilities and the cross sections show threshold behavior and the initial state selected rate constants are significantly dependent on the temperature.

Acknowledgments

The authors are grateful to Prof. G. G. Balint-Kurti for his guidance and Prof. Susana Gómez-Carrasco for providing the potential energy surface and Figure 1.

References

1. Walter, C. D.; Wagner, H. G. Ber Bunsenges Phys Chem 1983, 87, 403.
2. Sloan, J. J.; Watson, D. G.; Williamson, J. M.; Wright, S. J Chem Phys 1981, 75, 1190.
3. Bradforth, S. E.; Arnold, D. W.; Metz, R. B.; Weaver, A.; Neumark, D. M. J Phys Chem 1991, 95, 8066.
4. Dixon, R. N.; Tachikawa, H. Mol Phys 1999, 97, 195.
5. Gómez-Carrasco, S.; González-Sánchez, L.; Aguado, A.; Paniagua, M.; Roncero, O.; Hernández, M. L.; Alvariño, J. M. Chem Phys Lett 2004, 383, 25.
6. Gómez-Carrasco, S.; González-Sánchez, L.; Aguado, A.; Roncero, O.; Alvariño, J. M.; Hernández, M. L.; Paniagua, M. J Chem Phys 2004, 121, 4605.
7. González-Sánchez, L.; Gómez-Carrasco, S.; Aguado, A.; Paniagua, M.; Hernández, M. L.; Alvariño, J. M.; Roncero, O. Mol Phys 2004, 102, 2381.
8. Gómez-Carrasco, S.; Roncero, O. J Chem Phys 2006, 125, 054102.
9. Gogtas, F. J Comput Chem 2008, 29, 1889.
10. Zhao, J.; Xu, Y.; Yue, D.; Meng, Q. Chem Phys Lett 2009, 471, 160.
11. Chu, T. S.; Zhang, H.; Yuan, S. P.; Fu, A. P.; Si, H. Z.; Tian, F. H.; Duan, Y. B. J Phys Chem A 2009, 113, 3470.
12. Gómez-Carrasco, S.; Roncero, O.; González-Sánchez, L.; Hernández, M. L.; Alvariño, J. M.; Paniagua, M.; Aguado, A. J Chem Phys 2005, 123, 114310-1.
13. Gómez-Carrasco, S.; Aguado, A.; Paniagua, M.; Roncero, O. J Chem Phys 2006, 125, 164321.
14. Gómez-Carrasco, S.; Aguado, A.; Paniagua, M.; Roncero, O. J Photochem Photobiol A 2007, 190, 145.
15. Goḿez-Carrasco, S.; Hernandez, M. L.; Alvariño, J. M. Chem Phys Lett 2007, 435, 188.
16. Gray, S. K.; Balint-Kurti, G. G. J Chem Phys 1998, 108, 950.
17. Mandelshtam, V. A.; Taylor, H. S. J Chem Phys 1995, 102, 7390.
18. Kroes, G. J.; Neuhauser, D. J Chem Phys 1998, 105, 8690.
19. Mandelshtam, V. A.; Taylor, H. S. J Chem Phys 1995, 103, 2903.
20. Vibok, A.; Balint-Kurti, G. G. J Phys Chem 1992, 96, 8712.
21. Gray, S. K.; Goldfield, E. M. J Chem Phys 2001, 115, 8331.
22. Gögtas, F.; Balint-Kurti, G. G.; Offer, A. R. J Chem Phys 1996, 104, 7927.
23. Hankel, M.; Balint-Kurti, G. G.; Gray, S. K. Int J Quantum Chem 2003, 92, 205.
24. Meijer, A. J. H. M.; Goldfield, E. M.; Gray, S. K.; Balint-Kurti, G. G. Chem Phys Lett 1998, 293, 270.
25. Bowman, J. M. J Phys Chem 1991, 95, 4960.
26. Bitterova, M.; Bowman, J. M. J Chem Phys 2000, 113, 1.
27. Miquel, I.; González, M.; Sayos, R.; Balint-Kurti, G. G.; Gray, S. K.; Goldfield, E. M. J Chem Phys 2003, 118, 3111.
28. Chen, R.; Guo, H. J Chem Phys 1996, 105, 3569.